Medical Image Segmentation Using Active Contours

Serdar Kemal Balci

Abstract— **Medical image segmentation allow medical doctors to interpret medical images more accurately and more efficiently. We aim to develop a medical image segmentation procedure in order to reduce medical doctors' data examination and interpretation time. Active contours provide a means to detect boundaries of desired objects in images. In this paper we use active contours based on level set methods to detect and segment structures in medical data. We first review the theory of three level set based active contour methods; namely, geodesic active contours, area minimizing flows and active contours without edges. We apply these methods to 2D/3D synthetic data and to an MRI data with the aim of segmenting the boundaries of brain and present the results.**

Index Terms— **Medical image segmentation, active contours, level set methods, geodesic active contours, area minimizing flow, active contours without edges.**

I. Introduction

As a consequence of progressive technological improvements in screening techniques, medical doctors are provided with medical images having higher resolution rates. Therefore, medical doctors spend an increasing part of their time on examining and interpreting medical images. By developing a medical image segmentation procedure we aim at reducing medical doctors' data examination and interpretation time. To segment regions of interest from a medical image we will use active contours based on level set methods.

Active contours, or snakes, as defined by Kass et al. [1] are curves defined within an image domain that can move under the influence of internal forces coming from within the curve itself and external forces computed from the image data. The essential idea is to evolve a curve or a surface under constraints from image forces so that it is attracted to features of interest in an intensity image. Snakes are widely used in many applications, including edge detection, shape modeling, segmentation, and motion tracking. In this paper we will use active contours to segment regions of interest in a medical image.

The active contour models in literature can be classified into two broad categories: parametric active contours [1] and geometric active contours [3]- [8], [10]- [14]. In Kass et al.'s first efforts on active contours, the main idea was to formalize the problem as an energy minimization one. They defined active contours as energy-minimizing splines guided by external constraint forces that pull them toward features such as lines and edges. They also define an internal energy term which is used to impose a smoothness constraint on the moving curve. Because of the way the contours move while the energy is minimized they call them snakes. Kass et al.'s classical active contour model is important as a first efforts on this problem; however, their approach has some drawbacks which were attempted to be solved by subsequent researchers. The classical approach faced some difficulties such as handling topological changes during evolution, lack of a parametrization independent energy definition, detecting nonconvex objects, sensitivity to initialization, numerical instabilities and resampling problems arising in solving the energy minimization problem.

Level set methods as introduced by Osher-Sethian [3] provided a framework in which new active contour models can be formed which overcame the problems associated with classical energy minimization approaches. The level set formulation is based on the observation due to Osher-Sethian [3] that a curve can be seen as the zero level set of a function in higher dimension. Level set methods provide an efficient and stable algorithm to solve curve evolution equations. If the curve motion can be expressed as a velocity along the normal direction of the curve, level set methods can offer several advantages. Firstly, changes in topology of the active contour are handled implicitly during the curve evolution. This is the main advantage of level set formulation as the topological changes should not be taken into account explicitly. Secondly, for numerical approximations, a fixed discrete grid in the spatial domain and finite-difference approximations for spatial and temporal derivatives can be used. A third advantage is that level set methods can be extended to any dimension which is not straightforward with the classical energy minimization schemes.

The geometric active contour models [3]- [8], [10]- [14] have made use of these advantages of level set formulation. Geometric active contour models are based on designing a speed term so that the evolving front gradually attains zero speed as it gets closer to the object boundaries and eventually comes to a stop. The speed term might depend on the boundary of the front while it can also make use of the information inside the region enclosed by the evolving front. Beginning from Osher and Sethian's [3] level set formulation, Caselles et al. [4] and Malladi et al. [5] formulated their active contour model directly in terms of level sets. Caselles et al. [4] introduced geometric active contour model which was followed by Malladi et al. [5]. Caselles et al. [4] and Malladi et al. [5] designed a proper speed function so as to drive the evolving contour to the object boundaries. They provided a numerically stable and efficient model immune to topological changes. However, the stopping term was not robust and hence could not stop the leakage of the boundaries and if the front propagated and crossed the goal boundary, then it could not come back. Caselles et al. [6], [7] introduced geodesic active contours model which was based on an intrinsic weighted Euclidean length and showed its correspondence to Kass et al.'s classical snake model. Caselles et al. [6], [7] enhanced Caselles [4] and

Serdar Kemal Balci is with the Department of Electrical and Electronics Engineering at Bogazici University. (e-mail: serdar.balci@gmail.com)

Malladi's model [5] by introducing an additional edge strength term. Aubert et al. [9] showed that geometric active contours unify the curve evolution framework with classical energy minimization techniques. Siddiqi et al. [10], [11] introduce an area based active contour model which minimizes a weighted area functional. Siddiqi et al. combine the weighted area minimizing flow with the weighted length minimizing flow of Caselles et al. [7] and Kichenassamy et al. [8]. They define an additional attraction force which can handle object boundaries having complex structures.

Boundary based level set methods provide efficient and stable algorithms to detect contours in a given image. They handle changes in topology and provide robust stopping terms to detect the goal contours. However, structures such as interior of objects, e.g. interior of discs are not segmented. Because of level set formulation the final contours are always closed contours. In addition, in images where the objects boundaries are noisy and blurry these methods face some difficulties. Some recent work in active contours by Chan and Vese [12], [13] consider these issues. The main idea is to consider the information inside the regions not only at their boundaries. Chan and Vese formulate their problem using area functionals and solve the problem using level set methods.

To segment regions of interest in medical images we emphasize methods based on level set methods due to their aforementioned advantages. We will briefly review the theoretical part of three level set based active contour models, namely geodesic active contours by Caselles et al. [7], area minimizing flow by Siddiqi et al. [10] and active contours without edges by Chan and Vese [13]. Then we will state the results of applying these methods on 2D/3D synthetic images and on a 3D MRI data in order to detect boundaries of brain. Also, for the sake of completeness we will provide a brief overview of Kass. et al.'s [1] classical active contour model.

The paper is organized as follows. In section II, we will first introduce the notation that is used throughout the paper. Then we will present the Kass et al.'s [1] classical active contour model, Caselles et al.'s [7]geodesic active contour model, Siddiqi et al.'s [10] area minimizing flow and Chan and Vese's [13] active contours without edges, respectively. In section III, we will state the results for the implemented methods, namely geodesic active contours, area minimizing flow and active contours without edges. We will present results for 2D synthetic data, 3D synthetic data and 3D MRI data, respectively. In the conclusion part, we will provide a brief comparison of the performance of the employed methods and state some remarks.

II. Theory: Active Contours

In the following sections we will use the following notation. Let C be the set of curves in R^2 given by:

$$C = \left\{ c : [a,b] \to \Omega, \;\; piecewise\; C^1, c(a) = c(b) \right\} \tag{1}$$

Also let c' and c'' denote the first and second derivatives of c, respectively:

$$\begin{aligned} c(q) &= (c_1(q), c_2(q)) \\ c'(q) &= \left(\tfrac{dc_1}{dq}, \tfrac{dc_2}{dq} \right) \\ |c'(q)| &= \sqrt{\left(\tfrac{dc_1}{dq} \right)^2 + \left(\tfrac{dc_1}{dq} \right)^2} \end{aligned} \tag{2}$$

and similar notation for c''. We also note that the extension to three dimensions is straightforward and can be given as

$$\begin{aligned} c(q) &= (c_1(q), c_2(q), c_3(q)) \\ c'(q) &= \left(\tfrac{dc_1}{dq}, \tfrac{dc_2}{dq}, \tfrac{dc_3}{dq} \right) \\ |c'(q)| &= \sqrt{\left(\tfrac{dc_1}{dq} \right)^2 + \left(\tfrac{dc_1}{dq} \right)^2 + \left(\tfrac{dc_1}{dq} \right)^2} \end{aligned} \tag{3}$$

We also define an edge detector function $g(\nabla I)$ which is a monotonic decreasing function. A typical choice for $g(\nabla I)$ is

$$g(\nabla I) = \frac{1}{1 + |g(\nabla I)|^i} \tag{4}$$

where i can be selected between $1 < i < \infty$. In our work we used $i = 2$ for all methods we implemented. $g(\nabla I)$ is primarily an edge detector function which takes small values on edges and large values on smooth regions. The particular choice of $g(\nabla I)$ in equation (4) enhances contours in an image while reducing noise.

A. Classical Active Contour Model

Kass, Witkin and Terzopulos gave the first efforts in formulating the boundary detection problem as an energy minimization one [1]. They define active contours as energy-minimizing splines guided by external constraint forces that pull them toward features such as lines and edges. In Kass et al.'s approach, boundary detection consists of matching a deformable model to an image by means of energy minimization. Although we did not implement Kass. et al's method, we state the results here for the sake of completeness.

Using Aubert and Kornprobst's notation [2] for the formulation of Kass et al's active contour model, the energy functional $J(c)$ to be minimized is given by:

$$J(c) = \underbrace{\alpha \int_a^b |c'(q)|^2 dq + \beta \int_a^b |c''(q)|^2 dq}_{internal\;\; energy} + \underbrace{\lambda \int_a^b g^2 \left(|\nabla I\left(c(q)\right)| \right) dq}_{external\;\; energy} \tag{5}$$

The first two terms in equation (5) are called internal energy and are used to impose a smoothness constraint. The first order term makes the curve act like a membrane and the second term makes it act like a thin plate. Setting $\beta = 0$ allows second order discontinuities at corners. Instead of being constant $\alpha,\ \beta$ can be selected to depend on the curve parameters as $\alpha(s)\ \beta(s)$ allowing the weight of smoothness constraints to change along the curve. The third term, called the external energy, attracts the curve toward the edges of the objects by taking smaller values at the object boundaries.

The Euler-Lagrange equations associated with $J(c)$ are a fourth order system:

$$\begin{cases} -\alpha c'' + \beta^{(iv)} + \lambda \nabla F|_c(c) = 0 \\ c(a) = c(b) \end{cases} \quad (6)$$

Where $F(c_1, c_2) = g^2\left(|\nabla I(c_1, c_2)|\right)$ and $c^{(iv)}$ is the fourth order derivative.

In Kass et al.'s [1] approach the main ideas was to formulate the problem as a minimization one. However, this approach has significant drawbacks. One of the drawbacks is that the functional $J(c)$ is not intrinsic. It depends on the parametrization of c. Different solutions can be obtained by changing the parametrization while preserving the same initial curve. Another drawback is that the model cannot handle changes in topology. It is not possible to detect multiple objects. In addition nonconvex objects cannot be detected efficiently. A third consideration is about the numerical problems arising in solving equations in (6). In order to solve the system of equations in (6) the curve is made to depend on an artificial parameter t (the time) which may cause numerical instabilities. A difficult task is the choice of a set of marker points for discretizing the parametrized curve. The sampling rate of the markers has to be changed during iterations in order to avoid numerical instabilities and false detections.

B. Level Set Methods

The equations in (6) can be solved by parametrizing the curve and discretizing the equations. However, this direct approach faces some numerical difficulties such as numerical instabilities and the need for sampling rate changes. Level set methods as introduced by Osher-Sethian [3] provide an efficient and stable algorithm to solve (6).

The active contour models introduced in this part will make use of flows governed by equations of the form:

$$\begin{cases} \frac{\partial}{\partial t} = FN \\ c(0, q) = c_0(q) \end{cases} \quad (7)$$

Equation (7) states that the curve $c(t, q)$ moves along its normal with a speed F, which may depend on t, c, c', c''. The level set formulation is based on the observation due to Osher-Sethian [3] that a curve can be seen as the zero level set of a function in higher dimension. For example, a curve in R^2 can be represented as the zero-level line of a function $R^2 \rightarrow R$. Suppose that there exists a function such that $u : R^+ \times R \rightarrow$ such that

$$u\left(t, c(t, q)\right) = 0, \ \forall q, \forall t \geq 0 \quad (8)$$

Then by differentiating (8) with respect to t, we get

$$\frac{\partial u}{\partial t} + \left\langle \nabla u, \frac{\partial c}{\partial t} \right\rangle = 0 \quad (9)$$

Setting the speed term in (7) into (9)

$$\frac{\partial u}{\partial t} + \langle \nabla u, FN \rangle = 0 \quad (10)$$

The unit normal is given as

$$N = -\frac{\nabla u}{|\nabla u|} \quad (11)$$

Putting this into (10)

$$\frac{\partial u}{\partial t}\left(t, c(t, q)\right) = F|\nabla u\left(t, c(t, q)\right)| \quad (12)$$

This equation is valid only for the zero-level set of u . But, Osher-Sethian show in [3] that u can be regarded as defined on the whole domain $R^+ \times \Omega$. Then the following PDE can be solved

$$\frac{\partial u}{\partial t}(t, x) = F|\nabla u\left(t, x\right)| \quad (13)$$

For $t > 0$ and $x \in \Omega$ if F is defined on the whole space. Then once u is calculated on $R^+ \times \Omega$ the curve c can be obtained by extracting the zero level set of u . The normal derivative is chosen to vanish on the boundary and u is initialized to be the signed distance function to the initial curve c_0. Then, Osher-Sethian [3] give the following final model:

$$\begin{cases} \frac{\partial u}{\partial t}(t, x) = F|\nabla u\left(t, x\right)| & for (t, x) \in]0, \inf[\times \Omega \\ u(0, x) = \bar{d}(x, c_0) & (\bar{d}\ signed\ distance) \\ \frac{\partial u}{\partial N} = 0 & for (t, x) \in]0, \inf[\times \Omega \end{cases} \quad (14)$$

If the curve motion can be expressed as a velocity along the normal direction of the curve, the model in (14) is useful from several points of view. Firstly, the evolving function $u(t, x)$ remains a function during evolution as long as F is smooth. However, the level set $u = 0$, so the front $c(t, q)$, may change topology, break, merge as u evolves. This is the main advantage of level set formulation as the topological changes should not be taken into account explicitly. Secondly, for numerical approximations, a fixed discrete grid in the spatial domain and finite-difference approximations for spatial and temporal derivatives can be used. A third advantage is that geometric elements of the front such as the normal vector and the curvature can be expressed with respect to u. In addition, level set methods can be extended to higher dimensions.

The following active contour models will make use of these advantages of level set formulation. Active contour models based on Osher-Sethian's [3] level set formulation are based on designing the speed function $F(t, c, c', c'')$ in (14) so that the evolving front gradually attains zero speed as it gets closer to the object boundaries and eventually comes to a stop. In addition, special stopping functions are designed in order to detect the contours more efficiently.

C. Geodesic Active Contours

Beginning from Osher and Sethian's [3] level set formulation, Caselles et al. [4], proposed the geometric active contour model. The model proposed by Caselles was based on equations (14), where they define a proper speed function F. The geometric active contour was given by solving:

$$\frac{\partial u}{\partial t} = \underbrace{g(|\nabla I|)}_{stopping\ term} \underbrace{(\kappa + \alpha)}_{curvature\ +\ constant} (|\nabla u|) \quad (15)$$

α is a constant and κ is the curvature term which is given by:

$$\kappa = div\left(\frac{\nabla u}{|\nabla u|}\right) \quad (16)$$

The curvature term κ imposes smoothness constraints on the curve. The constant term α makes the detection of nonconvex objects easier and it increases the speed of convergence. In fact α is chosen so that $\alpha + \kappa$ does not change sign. In literature, the term α is sometimes called the balloon force as it acts as a constant force pushing the curve from outside or inside depending on its sign.

$g(|\nabla I)$ is the stopping term which forces the evolving front to attain zero speed as it gets closer to the object boundaries. Caselles et al. [4] give $g(|\nabla I)$ as follows:

$$g(|\nabla I) = \frac{1}{1 + |G_\sigma * \nabla I|} \tag{17}$$

Where $|G_\sigma * \nabla I|$ is the convolution of the gradient of the image with a Gaussian kernel of standard deviation σ.

Caselles et al. [4] formulated their active contour model directly in terms of level sets. Thereby, they provided a numerically stable and efficient model that can handle to topological changes.

In a sequence of papers Caselles et al. [6], [7] introduced geodesic active contours model which is based on an intrinsic weighted Euclidean length. What makes the geodesic active contours an important model is its correspondance to Kass et al.'s [1] classical snake model. Caselles et al. [7] use the following energy functional introduced by Kass et al. [1]

$$J_1(c) = \alpha \int_a^b |c'(q)|^2 dq + \lambda \int_a^b g^2 \left(|\nabla I(c(q))|\right) \tag{18}$$

Using the functional in 18, Caselles et al. [7] arrive at another energy functional which is intrinsic, i.e. independent of parametrization:

$$J_2(c) = \int_a^b g\left(|\nabla I(c(q))|\right) |c'(q)| \tag{19}$$

If we compare $J_2(c)$ to the classical definition of a curve $\left(L = \int_a^b |c'(q)| dq\right)$ we observe that $J_2(c)$ can be seen as a new length by weighting the Euclidean length. The weight is $g\left(|\nabla I(c(q))|\right)$, which contains information regarding object boundaries. Caselles et al. [7] define a new metric for which they seek for geodesic, hence the name geodesic active contours.

Caselles et al. [6], [7] formulate the solution to (19) in terms of level sets and arrive at the following level set expression:

$$\frac{\partial u}{\partial t} = g(|\nabla I|)(\kappa + \alpha)(|\nabla u|) + \underbrace{\langle \nabla g, \nabla u \rangle}_{pull\ back\ term} \tag{20}$$

This equation is similar to equation (15) and has an additional term $\langle \nabla g, \nabla u \rangle$, which attracts the curve further to the boundary. If the front propagates and crosses the goal boundary, this force pulls it back to the desired location.

D. Weighted Area Gradient Flow

Siddiqi et al. [10] [11] introduce an area based active contour model which minimizes a weighted area functional given by

$$A(c) = -\frac{1}{2} \int_0^L g\left(|\nabla I|\right) \langle c(s), N \rangle ds \tag{21}$$

where L is the length of the curve, and $c(s)$ is the arc length parametrization of the curve and $g(|\nabla I|)$ is the weighting function as defined in equation (4). Then the area minimizing flow takes the following form:

$$\frac{\partial c}{\partial t} = \left(g\left(|\nabla I|\right) + \frac{1}{2} \langle c, \nabla g\left(|\nabla I|\right) \rangle \right) N \tag{22}$$

The level set representation of area minimizing flow is given by

$$\frac{\partial u}{\partial t} = \frac{1}{2} div \left[\begin{pmatrix} x \\ y \end{pmatrix} \left(g\left(|\nabla I|\right)\right) \right] |\nabla u| \tag{23}$$

where x and y are the (x, y) coordinates of the given image. Siddiqi et al. [11] then combine the weighted area minimizing flow in (23) with the Caselles et al.'s weighted length minimizing flow in equation (20). The combined equation in level set form is given by

$$\frac{\partial u}{\partial t} = \begin{cases} g(|\nabla I|)(\kappa + \alpha)(|\nabla u|) + \langle \nabla g, \nabla u \rangle + \\ \frac{\lambda}{2} div \left[\begin{pmatrix} x \\ y \end{pmatrix} \left(g\left(|\nabla I|\right)\right) \right] |\nabla u| \end{cases} \tag{24}$$

where λ is a constant. The term $div \left[\begin{pmatrix} x \\ y \end{pmatrix} \left(g\left(|\nabla I|\right)\right) \right] |\nabla u|$ provides additional attraction force when the front is in the vicinity of an edge.

E. Active Contours Without Edges

Geodesic active contours and area minimizing flows presented thus far provide efficient and stable algorithms to detect contours in a given image. The presented methods handle changes in topology and provide robust stopping terms to detect the goal contours. However, structures such as interior of objects, e.g. interior of discs are not segmented. Because of level set formulation the final contours are always closed contours. In addition, in images where the objects object boundaries are noisy and blurry these methods face some difficulties. Some recent work in active contours consider these issues.

There are some objects whose boundaries are not well defined through the gradient e.g smeared boundaries. Chan and Vese [12], [13] introduce a new active contour model, called "without edges". The main idea is to consider the information inside the regions not only at their boundaries. Chan and Vese define the following energy

$$F(\phi,\beta_1,\beta_2)=\left\{\begin{array}{l}\mu\underbrace{\int_\Omega\delta(\phi)|\nabla\phi|}_{length\ of\ c}+v\underbrace{\int_\Omega H(\phi)dxdy}_{area\ inside\ c}+\\ \lambda_1\underbrace{\int_\Omega|u_0-\beta_1|^2H(\phi)dxdy}_{fitting\ term\ I}+\\ \lambda_2\underbrace{\int_\Omega|u_0-\beta_2|^2\left(1-H(\phi)\right)dxdy}_{fitting\ term\ II}\end{array}\right. \tag{25}$$

where u_0 is the original image, β_1,β_2 are some constants and $H(\phi)$is given by:

$$H(\phi)=\left\{\begin{array}{ll}1 & if\ \phi\geq 0\\ 0 & if\ \phi<0\end{array}\right. \tag{26}$$

This model looks for the best approximation of image u_0 as a set of regions with only two different intensities (β_1 and β_2). One of the regions represents the objects to be detected (inside of c), and the other region corresponds to the background (outside of c). The snake c will be the boundary between these two regions. This model is related in spirit to the Mumford-Shah functional [14] , which can be given as

$$F_{MS}(c,u)=\left\{\begin{array}{l}\mu\ length(c)+v\ area\left(inside(c)\right)\\ \underbrace{\int_\Omega|u-u_0|^2dxdy}_{fitting\ term}\end{array}\right. \tag{27}$$

where u is the cartoon image approximating u_0 , u is smooth except for jumps on the set c of boundary curves and the contour c segment the image into piecewise constant regions. The method in (25) is a simple approximation to (27) in that only two subregions are allowed in which u is piecewise constant. So u for (25) can be written as

$$u=\beta_1H(\phi)+\beta_2\left(1-H(\phi)\right) \tag{28}$$

Returning to equation (25), the last two terms are fitting terms which guide the curve to the boundaries of the object. The first fitting term $F_1(c)$ gives the error resulting from approximating the original image inside c with β_1 and the second fitting term $F_2(c)$ gives the error resulting from approximating the original image outside c with β_2. The first two terms in (25) are smoothing terms which smooth out sharp corners of the evolving contour.

The solution can be obtained by approximating $H(\phi)$ and $\delta(\phi)$ and by solving the following three equations

$$\left\{\begin{array}{l}\beta_1=\frac{\int_\Omega u_0H(\phi)dx}{\int_\Omega H(\phi)dx}\left(\begin{array}{c}average\ of\\ u_0\ inside\ c\end{array}\right)\\ \beta_2=\frac{\int_\Omega u_0(1-H(\phi))dx}{\int_\Omega(1-H(\phi))dx}\left(\begin{array}{c}average\ of\\ u_0\ outside\ c\end{array}\right)\\ \frac{\partial\phi}{\partial t}=\delta(\phi)\left(\mu\ div\left(\frac{\nabla\phi}{|\nabla\phi|}\right)-|u_0-\beta_1|^2+|u_0-\beta_2|^2\right)\end{array}\right. \tag{29}$$

where the last term is the Euler-Lagrange of equation (25).

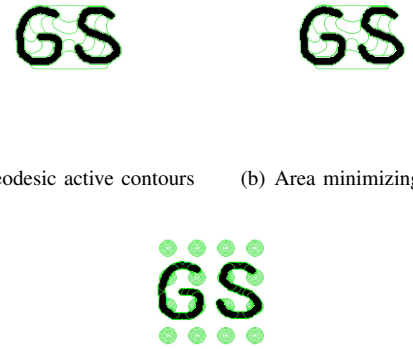

(a) Geodesic active contours (b) Area minimizing flow

(c) Active contours without edges

Fig. 1. Results for 2D synthetic image.

III. Results

We implemented geodesic active contours, area minimizing flows and active contours without edges for segmenting 2D/3D synthetic data and the boundaries of brain from an MRI data. To implement the level set methods we made use of a level set toolbox developed by Ian Mitchell [16]. We will present the segmentation results for 2D/3D synthetic data and 3D MRI data, respectively.

A. 2D-3D Synthetic Data

Figure 1 shows the results of applying geodesic active contours, area minimizing flows and active contours without edges to a 2D data. The steps of used algorithms can be seen in figures 4, 5, 6. The 2D synthetic data we used holds two letters of alphabet, "G" and "S", and is a monochromatic image having precisely two intensity values. Two letters are used to see how the active contours can handle the topological changes. In addition, "G" and "S" were chosen in order to test the capability of contours entering into concavities of the shapes.

As for the performance of the used methods, all methods were able to segment the two letters successfully. The results in figure 1 show that all methods were able to handle changes in topology as all of the methods are based on level set methods.

For geodesic active contours and area minimizing flows we selected the initial contour such that the region of interests fall inside the initial contour. We want to note that both methods are sensitive to initialization. Either the contour has to contain the two letters completely or the contour has to be completely inside the letters. In the first case we select $\alpha>0$ so that the contour contracts; in the second case $\alpha<0$ so that the contour inflates. In order to let the evolving contour enter into concavities of the letters we selected the balloon force term $|\alpha|>min(\kappa)$ so that the contraction(inflation) of the contour is assured. It can be stated that both geodesic active contours and area minimizing flows perform similarly. However, we can state that due to the additional attraction term in equation (24)

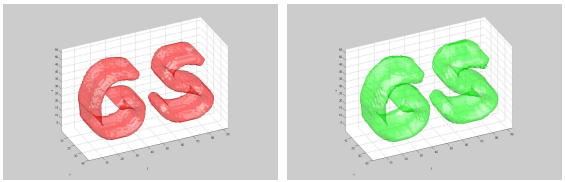

(a) Original image (b) Geodesic active contours

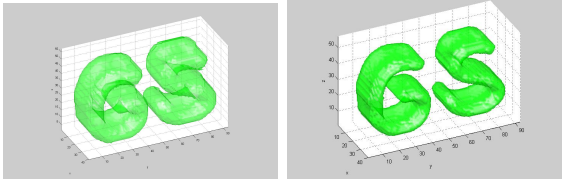

(c) Area minimizing flow (d) Active contours without edges

Fig. 2. Results for 3D synthetic image

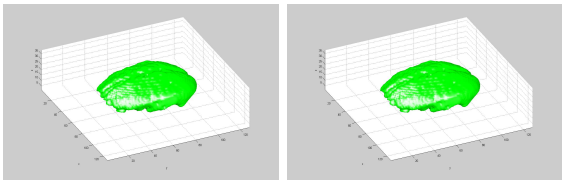

(a) Geodesic active contours (b) Area minimizing flow

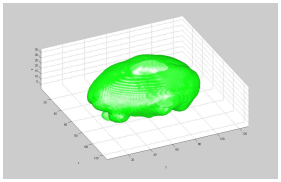

(c) Active contours without edges

Fig. 3. Results for segmenting the boundaries of brain from an MRI image

area minimizing flow performs slightly better than geodesic active contours. In addition, area minimizing flow is rather insensitive to the parameter α whereas α has to be tweaked for geodesic active contours.

Active contours without edges performed far more better than the other two methods in our 2D/3D synthetic data. This is due to the fact that active contours without edges try to approximate the given image using two intensity values, which is perfect for our setup. In addition, active contours without edges are insensitive to initialization. To show this property we initialized the contour to several circles distributed uniformly on the image (see figure 1(c)). It should be noted that some of the circles contracted whereas others inflated, which is not possible with the other two methods. Active contours without edges has the fastest convergence rate among all methods and its computational burden was the least among all methods. Area minimizing flow has a slightly better convergence rate than geodesic active contours; however, its computational burden was more than geodesic active contours due the additional attraction term in equation (24).

The synthetic 3D we used is similar to the 2D synthetic data we used before. It again consists of two letters, ”G” and ”S”, and is a monochromatic 3D image consisting only from two intensity values. The results for 3D synthetic data can be seen in figure 1 and the iterations can be seen in figures 7, 8, 9. Again the figures show how all methods were successful in segmenting the two letters and handling topological changes. All methods were easily extended to three dimensions using the same framework as in the two dimensions. As for the performance of the three methods in 3D, similar comments as in the 2D case apply to the 3D case.

B. MRI Data

We applied all the three active contour models to an MRI(128x128x38) image, the slices of which can be seen in figure 10, with the aim of segmenting the boundaries of brain. The results for this part can be seen in figure 3 and the intermediate steps for each algorithm can be seen in figures 11, 12, 13.

The comments made about topological changes, convergence rates, computational burden, parameter sensitivities and sensitivities to initialization in the previous section are still valid for the MRI data. However, some additional remarks can be made about the performance of the three methods.

All three methods were succesful in roughly locating the boundaries of the brain. In order to segment the boundaries of the brain, in geodesic active contours and area minimizing flows we started the contour completely inside the brain and inflated the contour till the boundaries. In segmenting the boundaries of the brain these two methods were more successful as they minimize an edge based functional. However, as the edges in the MRI image are quite blurry they smooth out the boundaries.

For the case of active contours without edges, again it was insensitive to initialization. However, it was not that successful in locating the boundaries of the brain. This is due to the fact that active contours without edges seek for the best approximation to the image using two intensity values. Therefore, in an MRI image, where the intensity values of different regions are close to each other and where there are blurry edges, active contours without edges necessarily introduce smoothing. What it does in fact is segmenting dark regions from bright ones.

IV. Conclusion

With the aim of developing a medical image segmentation procedure we used three level set based active contour models, namely geodesic active contours, area minimizing flows and active contours without edges. Firstly, we briefly stated the governing equations of these methods. Afterwards we applied these methods to 2D/3D synthetic data and to an MRI image with the aim of segmenting the boundaries of brain.

As all of the methods were based on level set methods, they handled topological changes during iterations implicitly and all of the methods were applicable to three dimensions. We can state that all methods have their cons and pros. Geodesic active contours and area minimizing flows differ only slightly in their performance. However, we can state that due to the

additional attraction term in equation (24) area minimizing flow performs slightly better than geodesic active contours. In addition, area minimizing flow is rather insensitive to the parameter α whereas α has to be tweaked for geodesic active contours.Area minimizing flow has a slightly better convergence rate than geodesic active contours; however, its computational burden was more than geodesic active contours due the additional attraction term in equation)24=.

Active contours without edges are formulated differently than the geodesic active contours or area minimizing flows. They seek for the best approximation to a given image using only two intensity values. Therefore, if the region of interest is significantly different in intensity values from other regions as in our synthetic 2D/3D data active contours without edges perform best among all methods we implemented. However, if the region of interest is defined through its edges as in the MRI data the results cannot be considered satisfactory. All in all, active contours without edges are insensitive to initialization, have a rather high convergence speed and its computational requirements are far more less than the geodesic active contours or area minimizing flows. In conclusion, according to our results level set based active contours are quite promising for medical image segmentation.

REFERENCES

[1] M. Kass, A. Witkin, D. Terzopoulos, "Snakes: Active contour models," *International Journal of Computer Vision*,vol. 1, pp. 321-331, 1988.

[2] G. Aubert and P. Kornprobst, *Mathematical Problems in Image Processing*. Germany: Springer Verlag, 2001, pp. 153-179.

[3] S.J. Osher and J.A. Sethian, "Fronts propagation with curvature dependent speed: Algorithms based on Hamilton-Jacobi formulations," *Journal of Computational Physics*, vol. 79, pp. 12-49, 1988.

[4] V. Caselles, F. Catte, T. Coll, and F. Dibos, "A geometric model for active contours," *Numer. Math.,* vol. 66, no. 1, pp. 1-31, 1993.

[5] R. Malladi, J. A. Sethian, and B. C. Vemuri, "Shape modeling with front propagation," *IEEE Trans. Pattern Anal. Machine Intell.,* vol. 17, pp. 158-175, Feb. 1995.

[6] V. Caselles, R. Kimmel, and G. Sapiro, "Geodesic Active Contours," *Proc. IEEE Int'l Conf. Computer Vision,*,pp. 694-699, 1995.

[7] V. Caselles, R. Kimmel, and G. Sapiro, "On geodesic active contours," *Int. J. Comput. Vis.*,vol. 22, no. 1, pp. 61-79, 1997.

[8] S. Kichenassamy, A. Kumar, P. Olver, A. Tannenbaum, and A. Yezzi, "Conformal curvatures flows: From phase transitions to active vision," *Arch. Rational Mech. Anal.*,vol. 134, no. 3, pp. 275-301, 1996.

[9] G. Aubert, L. Blanc-Feraud, "Some remarks on the equivalence between 2D and 3D classical snakes and geodesic active contours," *International Journal Of Computer Vision*,34(1), pp. 19-28, 1999.

[10] K. Siddiqi, Y. B. Lauriere, A. Tannenbaum, and S. W. Zucker, "Area and length minimizing flows for shape segmentation," *IEEE Trans. Image Processing*,vol. 7, pp. 433-443, 1998.

[11] K. Siddiqi, A. Tannenbaum, and S. W. Zucker, "Hyperbolic smoothing of shapes," *Proc. 6th Int. Conf. Comput. Vision (ICCV)*,vol. 1, Bombay, India, 1998, pp. 215-221.

[12] T. Chan and L. Vese, "An Active Contour Model without Edges," *Proc. Int'l Conf. Scale-Space Theories in Computer Vision*,pp. 141-151, 1999.

[13] T. Chan and L. Vese, "Active contours without edges," *IEEE Trans. Image Processing*,vol. 10(2), pp. 266-277, 2001.

[14] D. Mumford and J. Shah, "Optimal approximation by piecewise smooth functions and associated variational problems," *Commun. Pure Appl. Math*,vol. 42, pp. 577-685, 1989.

[15] S. Osher, R. Fedkiw, *Level Set Methods and Dynamic Implicit Surfaces.* New York: Springer Verlag, 2003, pp. 119-138.

[16] Ian Mitchell, "A Toolbox of Level Set Methods: version 1.0," *http://www.cs.ubc.ca/ mitchell/ToolboxLS/*, (email: mitchell@cs.ubc.ca), 9/2006.

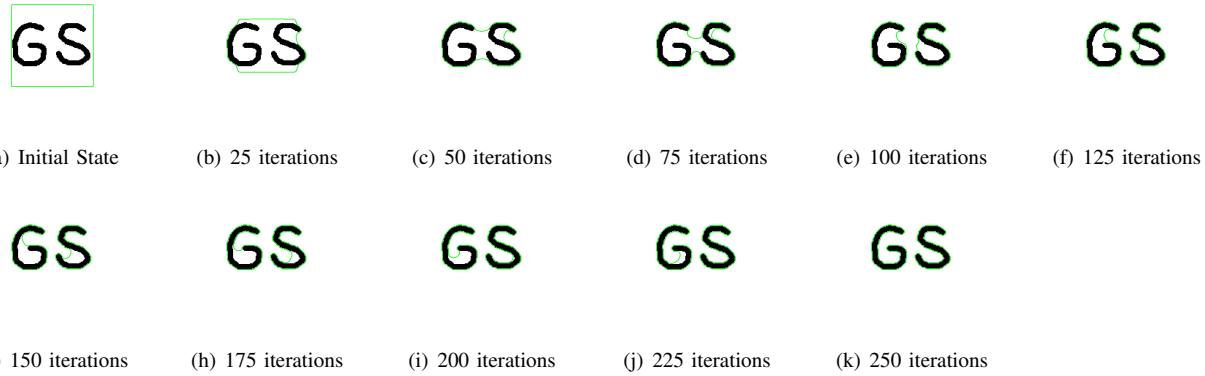

(a) Initial State (b) 25 iterations (c) 50 iterations (d) 75 iterations (e) 100 iterations (f) 125 iterations

(g) 150 iterations (h) 175 iterations (i) 200 iterations (j) 225 iterations (k) 250 iterations

Fig. 4. The results for the 2D synthetic image using geodesic active contours. Note the changes in topology. Observe the front entering into concave parts of the image. This is done by choosing $\alpha > min(\kappa)$

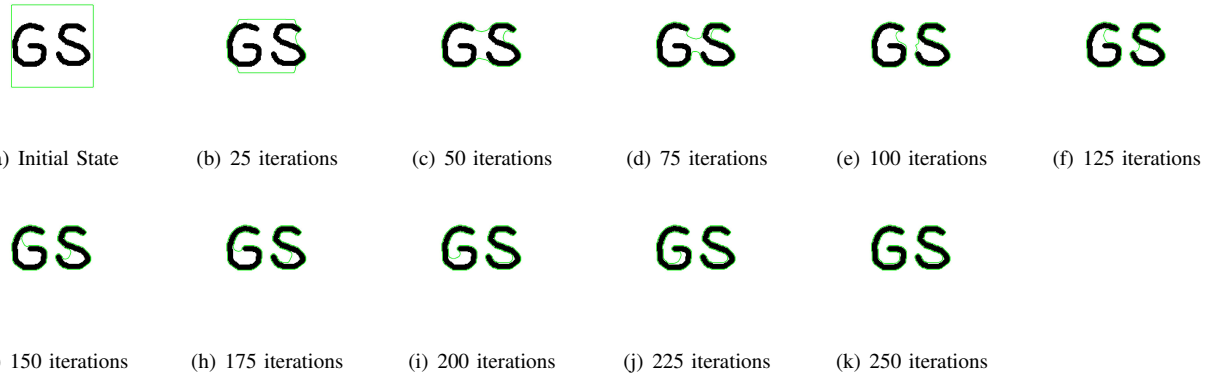

(a) Initial State (b) 25 iterations (c) 50 iterations (d) 75 iterations (e) 100 iterations (f) 125 iterations

(g) 150 iterations (h) 175 iterations (i) 200 iterations (j) 225 iterations (k) 250 iterations

Fig. 5. The results for the 2D synthetic image using area minimizing flows.

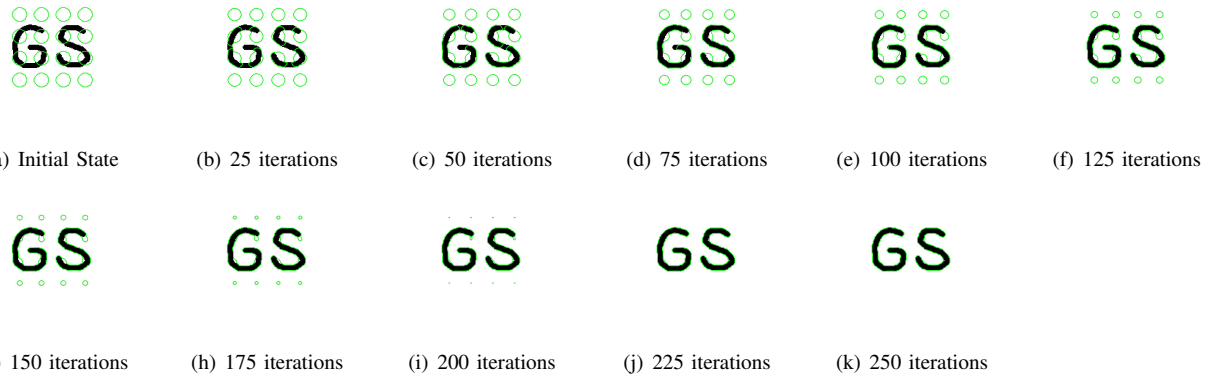

(a) Initial State (b) 25 iterations (c) 50 iterations (d) 75 iterations (e) 100 iterations (f) 125 iterations

(g) 150 iterations (h) 175 iterations (i) 200 iterations (j) 225 iterations (k) 250 iterations

Fig. 6. The results for the 2D synthetic image using active contours without edges.

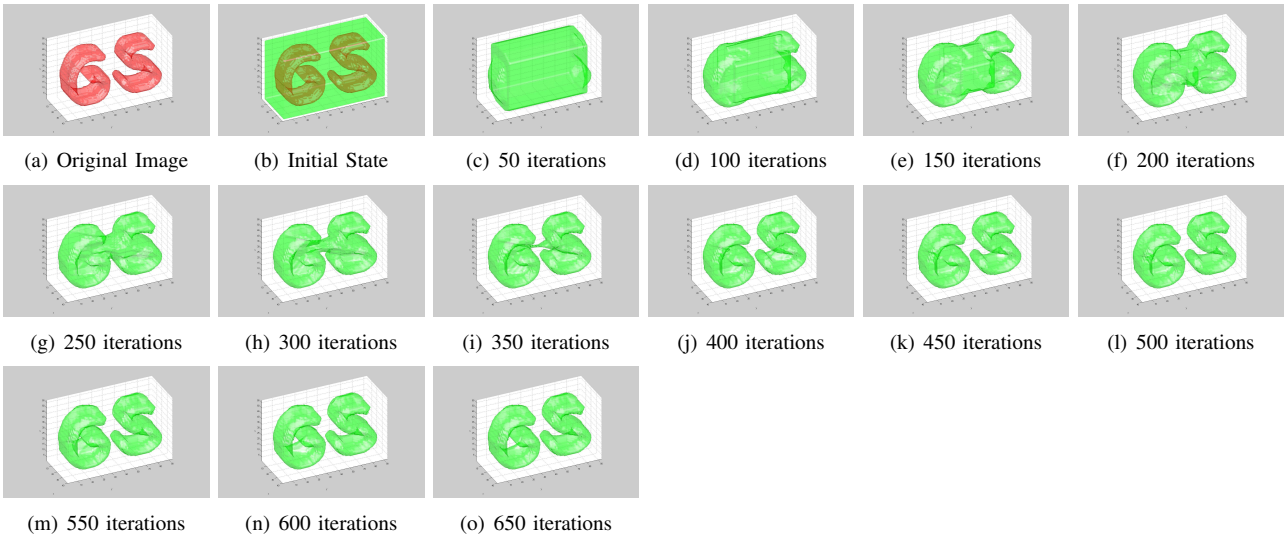

(a) Original Image (b) Initial State (c) 50 iterations (d) 100 iterations (e) 150 iterations (f) 200 iterations

(g) 250 iterations (h) 300 iterations (i) 350 iterations (j) 400 iterations (k) 450 iterations (l) 500 iterations

(m) 550 iterations (n) 600 iterations (o) 650 iterations

Fig. 7. The results for the 3D synthetic image using geodesic active contours

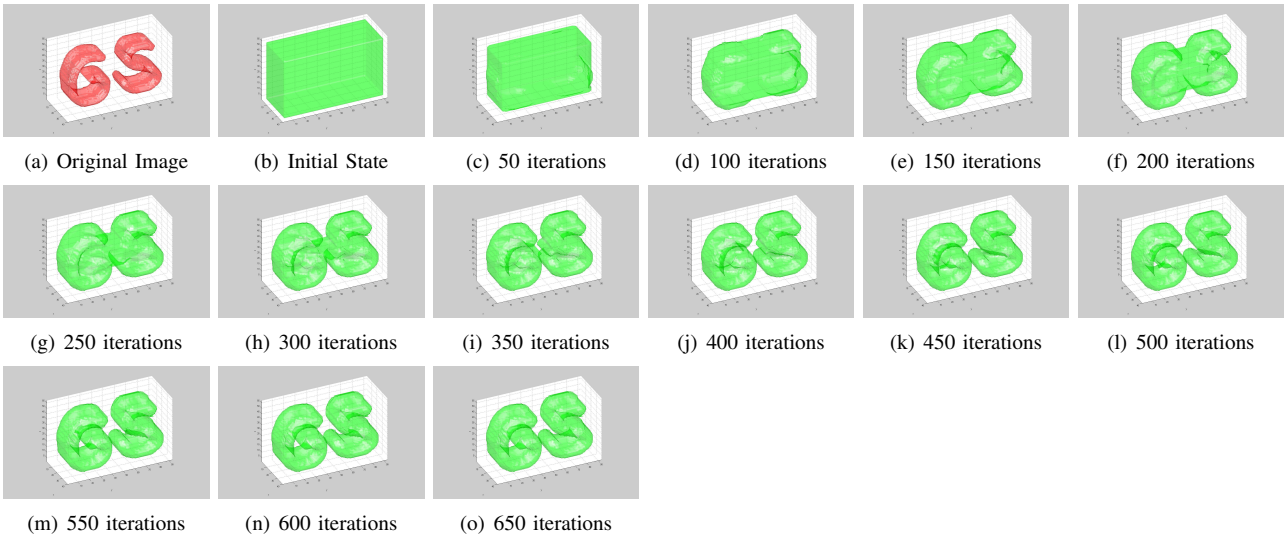

(a) Original Image (b) Initial State (c) 50 iterations (d) 100 iterations (e) 150 iterations (f) 200 iterations

(g) 250 iterations (h) 300 iterations (i) 350 iterations (j) 400 iterations (k) 450 iterations (l) 500 iterations

(m) 550 iterations (n) 600 iterations (o) 650 iterations

Fig. 8. The results for the 3D synthetic image using area minimizing flow

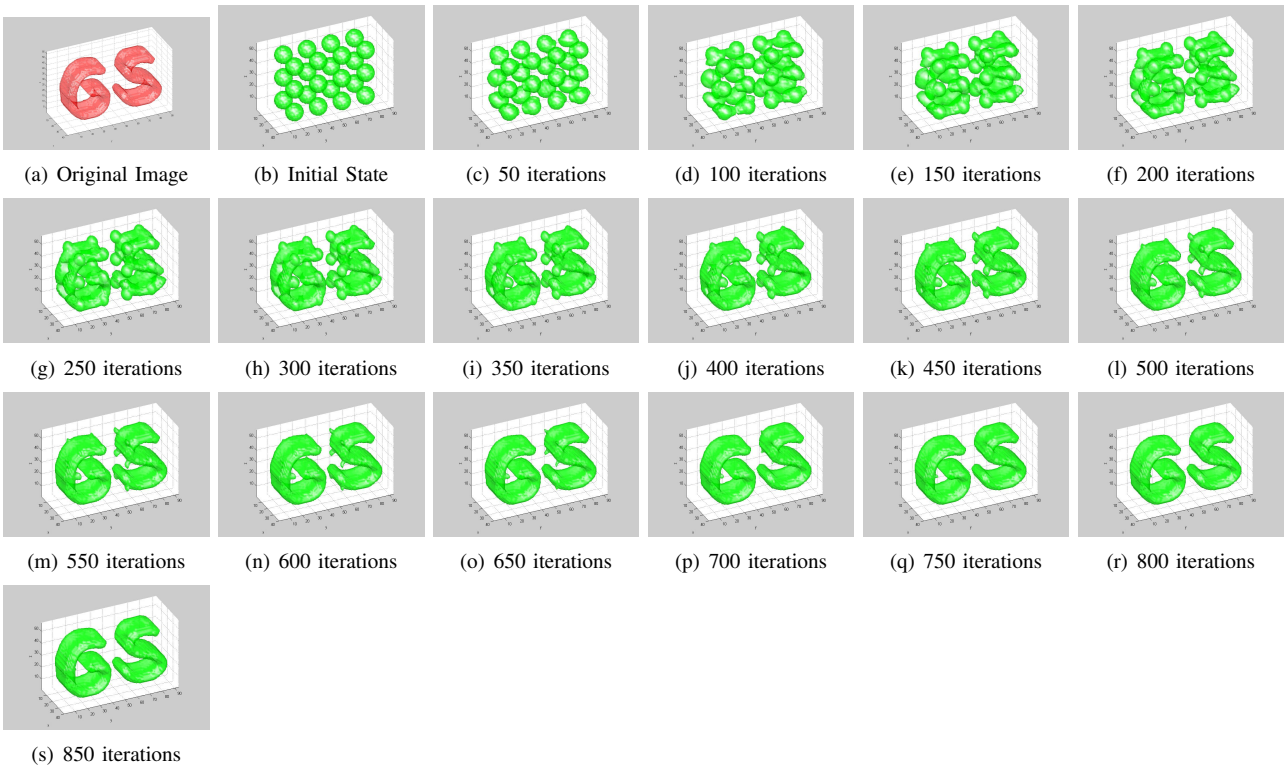

(a) Original Image (b) Initial State (c) 50 iterations (d) 100 iterations (e) 150 iterations (f) 200 iterations

(g) 250 iterations (h) 300 iterations (i) 350 iterations (j) 400 iterations (k) 450 iterations (l) 500 iterations

(m) 550 iterations (n) 600 iterations (o) 650 iterations (p) 700 iterations (q) 750 iterations (r) 800 iterations

(s) 850 iterations

Fig. 9. The results for the 3D synthetic image using active contours without edges

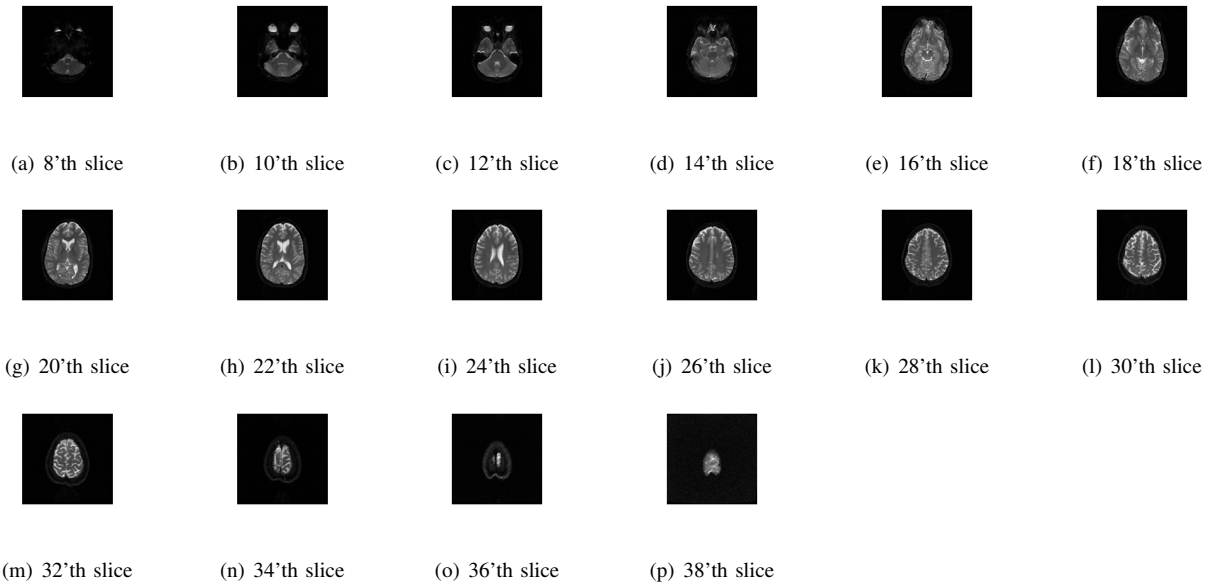

(a) 8'th slice (b) 10'th slice (c) 12'th slice (d) 14'th slice (e) 16'th slice (f) 18'th slice

(g) 20'th slice (h) 22'th slice (i) 24'th slice (j) 26'th slice (k) 28'th slice (l) 30'th slice

(m) 32'th slice (n) 34'th slice (o) 36'th slice (p) 38'th slice

Fig. 10. MRI slices

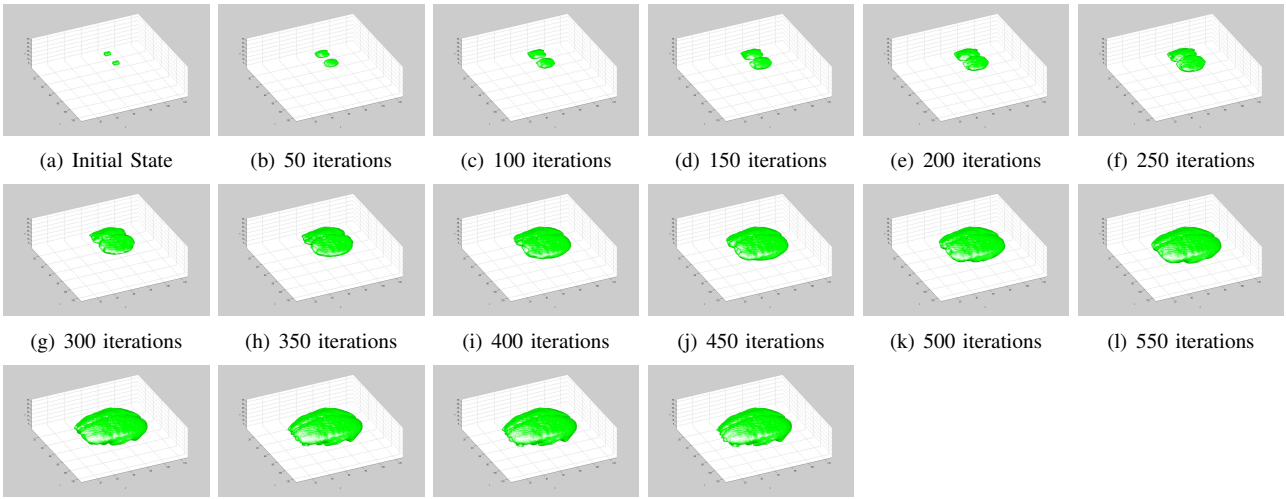

(a) Initial State (b) 50 iterations (c) 100 iterations (d) 150 iterations (e) 200 iterations (f) 250 iterations

(g) 300 iterations (h) 350 iterations (i) 400 iterations (j) 450 iterations (k) 500 iterations (l) 550 iterations

(m) 600 iterations (n) 650 iterations (o) 700 iterations (p) 750 iterations

Fig. 11. The results for segmenting the boundaries of brain from an MRI image using geodesic active contours

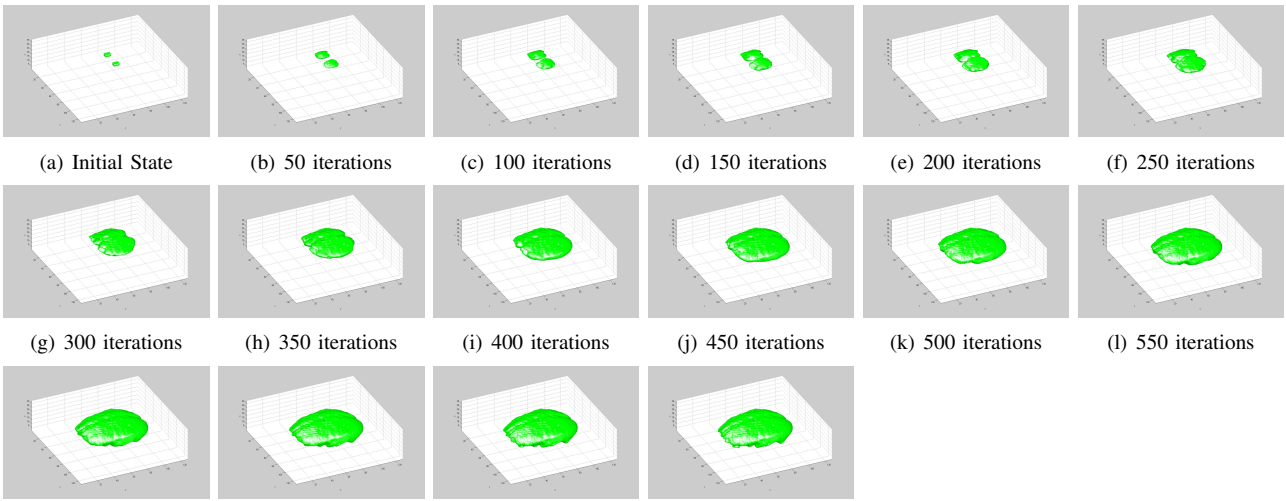

(a) Initial State (b) 50 iterations (c) 100 iterations (d) 150 iterations (e) 200 iterations (f) 250 iterations

(g) 300 iterations (h) 350 iterations (i) 400 iterations (j) 450 iterations (k) 500 iterations (l) 550 iterations

(m) 600 iterations (n) 650 iterations (o) 700 iterations (p) 750 iterations

Fig. 12. The results for segmenting the boundaries of brain from an MRI image using area minimizing flow

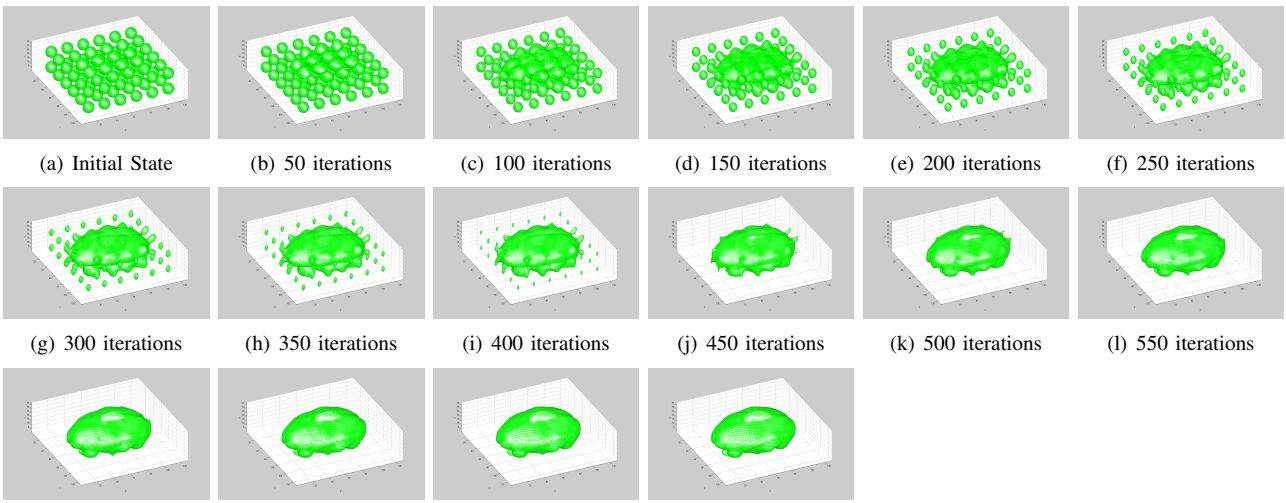

(a) Initial State (b) 50 iterations (c) 100 iterations (d) 150 iterations (e) 200 iterations (f) 250 iterations

(g) 300 iterations (h) 350 iterations (i) 400 iterations (j) 450 iterations (k) 500 iterations (l) 550 iterations

(m) 600 iterations (n) 650 iterations (o) 700 iterations (p) 750 iterations

Fig. 13. The results for segmenting the boundaries of brain from an MRI image using active contours without edges